



LAWRENCE  
LIVERMORE  
NATIONAL  
LABORATORY

# A Statistical Approach to Screening Isotopic Signatures in Monitoring for Underground Nuclear Explosions

C. R. Carrigan, Y. Sun, E. Herbold, T. Antoun

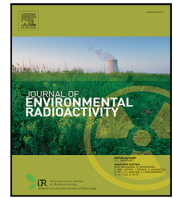
November 14, 2024

Journal of Environmental Radioactivity

## **Disclaimer**

---

This document was prepared as an account of work sponsored by an agency of the United States government. Neither the United States government nor Lawrence Livermore National Security, LLC, nor any of their employees makes any warranty, expressed or implied, or assumes any legal liability or responsibility for the accuracy, completeness, or usefulness of any information, apparatus, product, or process disclosed, or represents that its use would not infringe privately owned rights. Reference herein to any specific commercial product, process, or service by trade name, trademark, manufacturer, or otherwise does not necessarily constitute or imply its endorsement, recommendation, or favoring by the United States government or Lawrence Livermore National Security, LLC. The views and opinions of authors expressed herein do not necessarily state or reflect those of the United States government or Lawrence Livermore National Security, LLC, and shall not be used for advertising or product endorsement purposes.



# A statistical approach to screening isotopic signatures in monitoring for underground nuclear explosions

Charles R. Carrigan<sup>a,b,\*</sup>, Yunwei Sun<sup>b</sup>, Eric B. Herbold<sup>b</sup>, Tarabay Antoun<sup>b</sup>

<sup>a</sup> Stratify L.L.C./M.H. Chew Associates, Livermore, CA 94550, USA

<sup>b</sup> Lawrence Livermore National Laboratory, Livermore, CA 94550, USA

## ARTICLE INFO

### Keywords:

Radioactive decay  
Transport  
Underground nuclear explosion  
Noble gas  
Xenon isotopic evolution

## ABSTRACT

The ability to differentiate between atmospheric radionuclide signatures from underground nuclear explosions (UNEs) and signals from other sources, such as medical isotope-production facilities and nuclear reactors, can be critical to the detection and monitoring of unannounced, low-yield nuclear events. Signatures having anomalously high amplitudes, compared to background levels, remain the best indicator in screening for a UNE. However, isotopic composition can further validate a suspected UNE signature, but separation from any atmospheric background composition is first necessary. To date, evaluating the challenges of performing this separation has typically involved comparing an observed background with a highly idealized deterministic model of radioxenon signature production by a UNE that does not consider the influence of post-detonation chemical/physical processes in the detonation cavity or the subsequent gas transport mechanisms that can also affect the isotopic composition of the detected gas signature. In addition, purely deterministic models, as previously employed, overlook the uncertainty inherent in estimating critical parameters characterizing the UNE and its detonation environment. In this paper, we create detailed, multi-parameter models of radionuclide evolution using the widely accepted England and Rider post-detonation radionuclide decay-chain network coupled to detailed models simulating physical production and transport processes affecting the gas signature. Because these models are governed by uncertain parameters including barometric fluctuations, realistic ranges of variation for each of the parameters influencing isotopic composition are then defined. A Latin-Hypercube sampling approach is used to obtain a random distribution of isotopic production and gas transport results associated with a given value of each parameter. We apply these results to background histories of two stations, one providing 4-isotope background measurements and the other providing two-isotope measurements associated with the 2013 DPRK announced UNE.

## 1. Introduction

Screening radionuclide signatures produced by underground nuclear explosions (UNEs) from the atmospheric radionuclide background (ARB) is particularly challenging for several reasons. While extensive atmospheric measurements obtained over the last decade exist characterizing ARB at many different locations, only rarely have signatures clearly associated with UNEs been captured by the International Monitoring System (IMS) of the Comprehensive Test Ban Treaty Organization. This lack of available UNE isotopic data for developing well-documented UNE signature examples has led to substituting the predictions of idealized models of isotopic evolution to allow comparison with the actual isotopic background measurements. However, these deterministic UNE signature models represent an endmember and idealized case in which all gases in the detonation cavity are assumed well-mixed and confined within the cavity during their compositional

evolution. Such assumptions affect the time-dependent isotopic compositions (*i.e.*, isotopic ratios) within the cavity (Carrigan et al., 2020) and are known not to hold rigorously. For example, drilling back into post-detonation UNE cavities indicates that condensates of parent radionuclides of isotopic xenon may be lost to both the molten rock puddle forming at the bottom of the chamber as well as to the surfaces of the rubblized containment zone at early times during isotopic xenon evolution (Cassata et al., 2014; Carrigan et al., 2020). Simulations of the condensation and subsequent separation of parental radionuclides from the overlying gas phase in the post-detonation cavity along with gas leakage from the cavity have been shown to potentially influence the composition of gases detected at the surface (Carrigan et al., 2020, 2022). More detailed isotopic evolution models have been developed

\* Corresponding author at: Stratify L.L.C./M.H. Chew Associates, Livermore, CA 94550, USA.  
E-mail address: [carrigan1@llnl.gov](mailto:carrigan1@llnl.gov) (C.R. Carrigan).

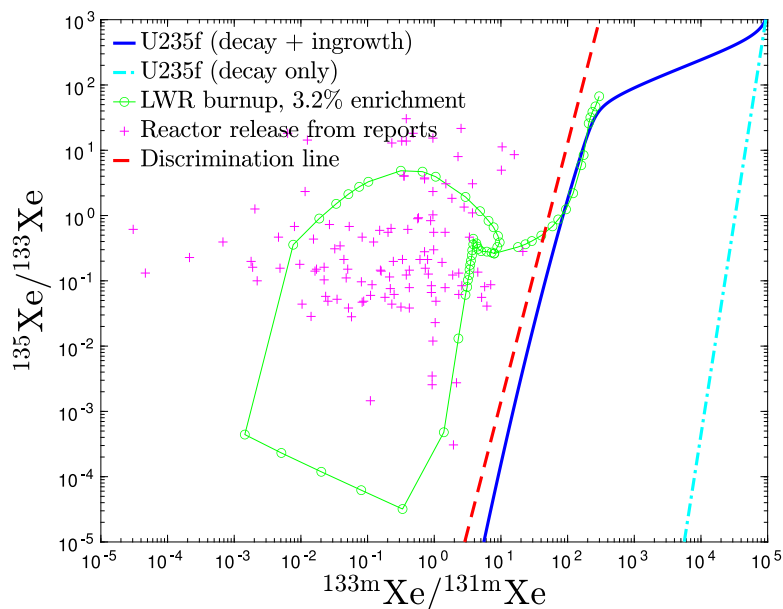


Fig. 1. The four-isotope chart, sometimes referred to as a Kalinowski plot, is divided into a background zone (left side) and a nuclear test zone (right side) of the “Discrimination Line” representing an arbitrary boundary between the zones. The magenta crosses represent individual atmospheric measurements while the continuous green line represents the time-varying output of a Light Water Reactor (LWR). The curves to the right of the “Discrimination Line” represent the idealized evolution of radioxenon for the U235f decay chain. The plot is taken from Carrigan et al. (2020). LWR data is replotted from Kalinowski et al. (2010). (For interpretation of the references to color in this figure legend, the reader is referred to the web version of this article.)

that introduce additional parameters compared to the simpler well-mixed and fully contained model (Carrigan et al., 2022) including further refinement of the post-detonation condensation process of relevant isotope precursors (Bourdon and Pili, 2023). Unfortunately, most UNE-defining parameters (e.g., depth, nuclear yield, containment zone rock and soil characteristics, etc.) tend to be poorly known or not known at all, and only estimates of their ranges are typically possible during the monitoring process. The migration of gases from the post-detonation cavity is responsible for further modification of the signature relative to the idealized, well-mixed and perfectly contained case (Carrigan et al., 2022). However, detailed models attempting to characterize transport of gases across the zone of containment introduce further uncertainty owing to unknown values of the new parameters required to characterize the different modes of leakage to the surface.

While deterministic models may be helpful for understanding how cavity and containment zone processes can affect isotopic signatures, it is apparent from the degree of parametric uncertainty that a more statistical approach must be considered if one is to reach any meaningful conclusions about the potential impact of the isotopic background on screening for hypothetical UNE signatures. In this paper we develop probabilistic models for estimating the range of possible radioxenon gas signatures for each considered parameter that contributes to defining a particular UNE.

One of the goals of this study is to estimate the likelihood that the signature of a UNE, defined by a given set of parameters, will fall into or intersect the zone on a xenon isotopic chart that is defined or populated by the presence of background “noise”. What has become a classic representation of the relationship between atmospheric background and a UNE signature is the four-isotope plot shown in Fig. 1 based on the earlier work of (Kalinowski et al., 2010).

The solid blue line in Fig. 1 represents the temporal evolution of radioxenon ratios, which arise from the ingrowth due to the decay of radioactive precursors, starting at time  $t = 0$ . This point corresponds to the intersection of the solid and dot-dashed lines. The dot-dashed cyan line illustrates the evolution of the isotopic xenon produced immediately at  $t = 0+$ , referred to as the “independent yield (IY)” of radioxenon isotopes. The righthand side of the figure is based entirely upon the isotopic decay of four isotopes, as determined by England

and Rider (1994). For the decay-chain model of England and Rider to accurately represent the isotopic evolution of gases in the UNE detonation cavity, it requires potentially unrealistic assumptions of a well-mixed and closed cavity (Carrigan et al., 2020). These assumptions that will be discussed in further detail.

The England and Rider model for UNE isotopic evolution, which relies solely on the decay of precursors of the four xenon isotopes in the cavity, is also subject to some uncertainty. Sloan et al. (2016) demonstrated that uncertainty in the initial concentrations of radioactive precursors, or parents of the relevant xenon isotopes, is propagated along the ingrowth curve. This propagation results in a zone on the four-isotope plot that has a 95% probability of containing the xenon isotopic ratios (see Fig. 2).

More realistic models of signature evolution in the post-detonation cavity, which introduce additional uncertain parameters, have been considered by several authors (Carrigan et al., 2016, 2020, 2022; Bourret et al., 2021; Bourdon and Pili, 2023). In this paper, we adopt a probabilistic approach to screening UNEs and utilize well-known decay-ingrowth networks, specifically, their structure, half-lives, branching factors, and independent yields, based on the England and Rider database. For future studies, updated nuclear fission databases (e.g., Plompen et al. (2020)) should be considered in case-specific analyses, provided that they demonstrate reduced uncertainties. In our models, the post-detonation precursor rainout process is simplified as a Heaviside function of temperature, using a temperature profile simulated according to Olsen (1967). When better hydrodynamic information becomes available, other factors, such as pressure and oxygen concentrations, should be incorporated into the calculations for the condensation and rainout of radioxenon precursors.

Subsurface gas transport has also benefited from the development of more sophisticated models (Lowrey et al., 2013; Sun and Carrigan, 2014; Sun et al., 2015; Jordan et al., 2015; Carrigan et al., 2016, 2022; Bourret et al., 2019; Harp et al., 2020). Collectively, these papers summarize the current understanding of the complex interactions that may potentially occur within the detonation cavity and during transport across the overlying containment zone, leading to deviations from the England and Rider-based model. In what follows, we will explore the

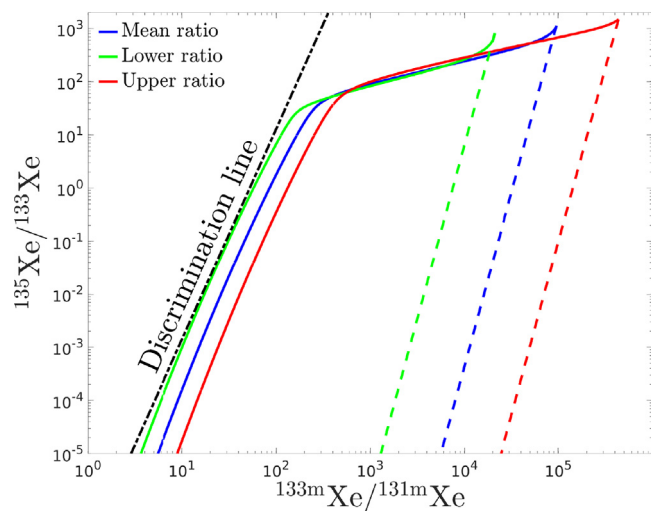


**Fig. 2.** The 4-isotope plot illustrating the bounds of uncertainty in the xenon isotopic ingrowth curve that is propagated by estimated errors in initially produced relative concentrations of radioxenon precursors and other decay-chain parameters. (For interpretation of the references to color in this figure legend, the reader is referred to the web version of this article.)

Source: Modified from Sloan et al. (2016).

effect of parametric uncertainty on the probability of obtaining a specific radioxenon signature at the point of release into the atmosphere. This uncertainty arises not only from a lack of information regarding the details of test-site engineering and emplacement parameters of an unannounced UNE, such as yield, fission type, and depth of detonation, but also from significant uncertainties related to the containment zone's host rock and soil properties, including permeability, saturation, porosity, and natural and post-detonation fracturing.

## 2. Methods

### 2.1. Analytical model of source evolution

The closed-form solution simulates time-dependent mass exchanges among the UNE cavity, melt puddle, and surrounding host rock (Sun et al., 2021, 2023). The model calculates xenon production associated with the independent yield and ingrowth chain reactions, while also tracking xenon fluxes from the cavity into the host rock, including the underlying rock melt. The physical processes involved include:

1. thermally induced condensation (rainout) of refractory iodine precursors from cavity to rock melt,
2. seepage of cavity gases into a fractured containment zone,
3. back diffusion from melt puddle to the cavity, and/or
4. prompt venting of cavity gases to ground surface.

The independent yields provided by England and Rider (1994) serve as the initial conditions in the source evolution model. However, the uncertainties associated with independent yield, expressed as a multiplier between 0 and 1, represent the 11th uncertain input (see Table 1). A value of zero indicates no uncertainty, while a value of one corresponds to the uncertainty published by England and Rider (1994). The xenon fluxes calculated from the source evolution model will be utilized as source terms in the subsurface transport models (see Fig. 3).

### 2.2. Numerical model of subsurface transport

Nonisothermal multiphase reactive transport, represented by mass and energy balance equations for water, air, and radionuclides in liquid, gas, and non-deformable solid phases, is simulated using the

LLNL NUFT code (Nitao, 1998; Hao et al., 2012; Sun et al., 2012; Sun and Carrigan, 2016). As illustrated in Fig. 3 (yellow box), xenon isotopes produced from UNEs and simulated using the source-evolution model serve as source-term inputs to the subsurface transport models.

Based on our previous study, we consider convection, dispersion, diffusion, gas dissolution in liquid, and gas sorption on solid porous media. Phase change, driven by UNE residual heat, and barometric pumping are the major driving forces transporting xenon isotopes from a UNE source to the ground surface. The model grid is generated according to uncertain inputs, such as yield, rock type, depth of burial, and initial rock saturation. A dual-permeability model is employed to account for fractures and the rock matrix.

Latin hypercube sampling (McKay et al., 1979) is used to generate sample points in the 11-dimensional parametric space. Numerical models of subsurface transport are then developed and executed at these sample points. The main outputs considered are the xenon isotopic concentrations at the ground surface and the xenon fluxes to the atmosphere, integrated over the entire surface area of the study domain.

### 2.3. Uncertainty quantification

We utilized the LLNL PSUADE (Tong, 2005) non-intrusive, sampling-based approach to generate probability density functions for xenon concentrations and fluxes, as well as to conduct sensitivity analyses. This sampling-based method is employed to establish the relationship between model outputs and uncertain inputs. System parameters were selected based on previous studies regarding their influence on isotopic signatures in the cavity and at the ground surface. Table 1 lists all considered parameters and their respective ranges.

The Sobol' sensitivity analysis (Sobol', 1990), which is calculated based on the decomposition of model output variance into components corresponding to the variances of uncertain inputs, determines the contribution of each uncertain input and its interactions with other uncertain inputs to the variance of the overall model output of interest, such as xenon concentrations and fluxes. The total sensitivity of the output (e.g., xenon concentrations) to uncertain inputs is computed as the sum of all sensitivity indices, including all interactive effects (Tong, 2005). Technical details of the Sobol' sensitivity approach can be found in Saltelli et al. (2008). It should be noted that the Sobol' analysis is used here simply to learn what parameters are most important in determining the outcome of a simulation. No attempt is made to consider only the most important parameters. All eleven parameters are considered in this study.

To estimate the range of isotopic compositions, our cavity evolution and barometric gas migration models (Carrigan et al., 2022; Sun et al., 2023) require specifying the values of 11 parameters, along with a record of barometric pressure fluctuations at the surface. To understand the effects of varying these 11 parameters, we populated 7,200 sets of sample points in the parameter space, each set defining a model run, and generated an equal number of source-term models and subsurface transport models using the corresponding sample points.

Xenon concentrations derived from source-evolution models in the cavity, melt puddle, and/or surrounding host rock are treated as uncertain outputs. Similarly, the xenon fluxes from the cavity to the host rock, which are also uncertain outputs of the source models, serve as uncertain inputs to the subsurface transport models. The xenon concentrations at the ground surface, along with their fluxes to the atmosphere, are utilized to calculate the probability that these quantities will fall within certain ranges relevant to the detection of a UNE.

The eleven uncertain inputs (nuclear yield, rock type, detonation depth, chimney height/cavity diameter or ratio, fracture permeability, initial rock saturation, post-detonation source temperature following cavity collapse, early-time condensate rainout rate, back diffusion rate, gas seepage rate, and uncertainties of independent yields) are assumed

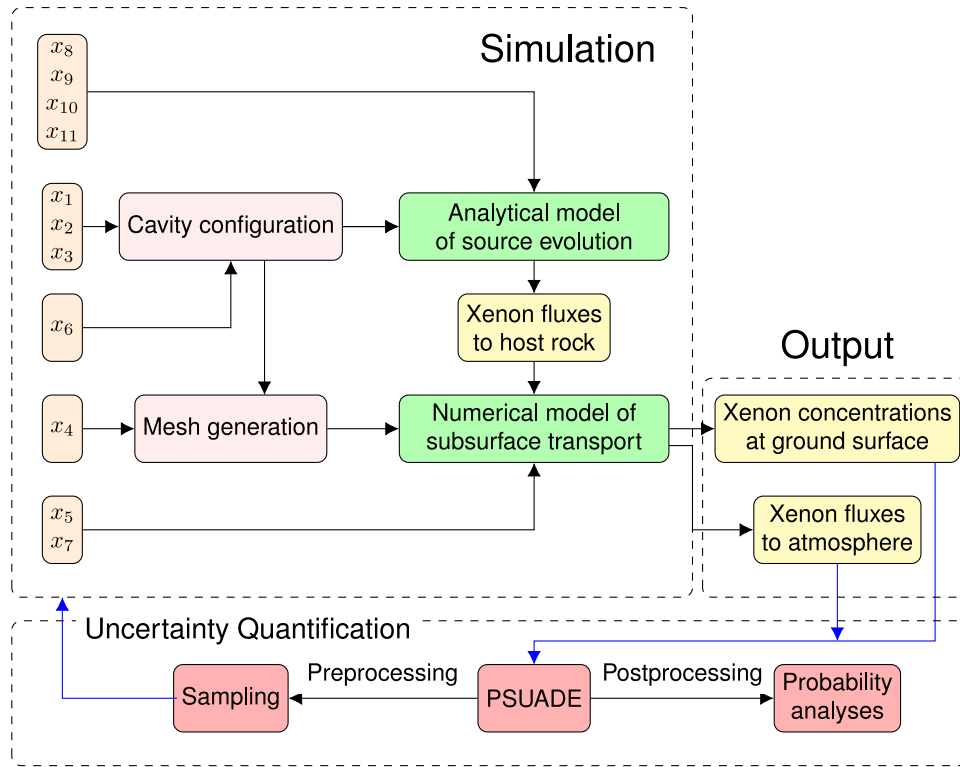


**Fig. 3.** Flowchart of model simulations and uncertainty quantification. The uncertain inputs  $x_i$ ,  $i = 1, 2, \dots, 11$ , are defined in Table 1. Initially, PSUADE performs preprocessing by selecting 7,200 parameter sets using a Latin hypercube approach. These parameter sets define conditions for both cavity evolution and the transport of gases across the containment zone. The output includes xenon concentrations at the surface and the fluxes into the atmosphere. In post-processing mode, PSUADE uses the model outputs to estimate the probability that the fluxes or concentrations will fall within a given range of values.

**Table 1**

Eleven parameters define the post-detonation cavity evolution and subsurface transport (seepage) of radionuclide isotopes. The tables illustrate the range of each parameter covered in the 7,200 simulations considered.

Parameter	Definition	Unit	Minimum	Maximum
$x_1$	Yield	[kt]	1.00	10.00
$x_2$	Rock type	[-]	51.31	77.66
$x_3$	Depth of burial	[m]	50.00	200.00
$x_4$	Chimney height/radius ratio	[-]	1.00	4.00
$x_5$	Fracture permeability	[m <sup>2</sup> ]	$1.0 \times 10^{-13}$	$1.0 \times 10^{-11}$
$x_6$	Initial saturation	[-]	0.50	0.99
$x_7$	Source temperature	[°C]	150.00	350.00
$x_8$	Rainout rate	[s <sup>-1</sup> ]	$1.0 \times 10^{-6}$	$1.0 \times 10^{-3}$
$x_9$	Diffusion rate	[s <sup>-1</sup> ]	$1.0 \times 10^{-6}$	$1.0 \times 10^{-4}$
$x_{10}$	Seepage rate	[s <sup>-1</sup> ]	$1.0 \times 10^{-7}$	$1.0 \times 10^{-5}$
$x_{11}$	Uncertainty, independent yields	[-]	0	1

to be uniformly distributed across an 11-dimensional space by generating sample points across the parameter space using the Latin hypercube method (Tong, 2005). A set of 7,200 source-term evolution models (Sun et al., 2021, 2023) and a set of 7,200 subsurface transport models (Sun and Carrigan, 2014) were developed on those sample points. Note that the rock-type parameter represents the compressibility of the rock during detonation and varies from a predominantly granite to tuff geology (Butkovich, 1974; Sun et al., 2023). The cavity configuration, which is simulated at each sample point using yield, rock-type parameter, depth of burial, the ratio of chimney height to cavity radius, and initial saturation (Butkovich, 1974), is used for generating its mesh file for the corresponding subsurface transport model.

Since the surface signature is time-dependent we will track it during the course of its evolution over a period of approximately two weeks, which corresponds to the time that monitoring may be required to

achieve a 90% probability of detection by the IMS (Medici, 2001; Schulze et al., 2000). Note that this represents only the probability that the isotopic source term, as released at the ground surface above the UNE will be separable from the background. In a subsequent paper, we will consider the effect of atmospheric transport along with the added parametric uncertainty associated with coupling subsurface and atmospheric simulations.

### 3. Results and analyses

#### 3.1. Effects of deviation from the idealized model of isotopic evolution

It is helpful to understand how each considered deviation from the assumption of a well-mixed and sealed cavity can potentially affect the ingrowth curve (Sun et al., 2023).

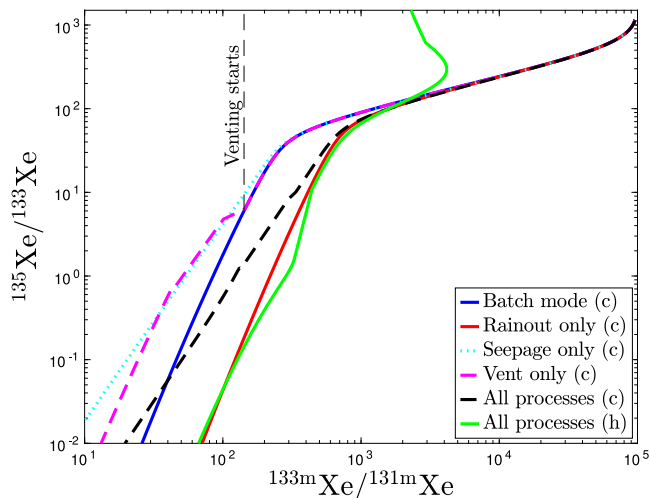


**Fig. 4.** Deterministic simulations conducted under varying cavity conditions during the post-detonation period. The England and Rider (Batch mode) case assumes an idealized, well-mixed, closed-cavity scenario (represented by the blue line). However, deviations from this well-mixed condition, caused by the rainout of condensing parent radionuclides of radioxenon, result in a shift of the ingrowth to the right (indicated by the red line). Additionally, leakage of cavity gas through the containment zone or seepage contributes to ingrowth, causing the radioxenon composition to shift to the left (as shown by the dotted cyan line), approaching the discrimination line in Fig. 1. Sudden high flow-rate venting (illustrated by the dashed magenta line) leads to ingrowth patterns similar to those observed in the seepage-only scenario. When all deviations from the ideal case are combined, the ingrowth within the cavity (represented by the black dashed line) is positioned between the rainout and gas-loss (seepage-only and vent-only) curves. Interestingly, the bulk composition of radioxenon that has escaped the cavity (depicted by the green line) closely resembles the rainout-only case for the selected parameters. All curves apply to the cavity environment (c) except for the green line which applies to host rock environment (h). (For interpretation of the references to color in this figure legend, the reader is referred to the web version of this article.)

Source: Replotted from Sun et al. (2023).

Fig. 4 illustrates the results on the 4-isotope chart, also called Multiple Isotope Ratio Chart (MIRC), of introducing different deviations from the idealized England and Rider based model. Assuming the idealized conditions of a well-mixed cavity yields the blue curve in this figure. If condensation of the more refractory radionuclide parents of isotopic xenon occurs followed by rainout or loss of those parents into the molten walls or puddle that forms in the cavity causing violation of the well-mixed assumption tends to result in migration of decay/ingrowth curve, here the red curve, towards the right side of the MIRC and away from the discrimination line shown in Fig. 1. On the other hand, seepage or leakage of gas from the cavity tends to shift the ingrowth curve to the left towards the discrimination line. More dramatic loss of gases by venting can also have a similar effect to seepage in shifting the curve towards the left. The magnitudes of these effects taken together can produce a black-dashed isotopic-ingrowth curve representing the cavity radioxenon composition while the green curve is the bulk composition of all gases released by seepage into the overlying containment regime outside of the cavity. The results of Fig. 4 are clearly deterministic and the relative positions of the different curves partially depend on the particular parameters chosen. Such deterministic simulations can provide insight into how each cavity or subsurface process might modify the ingrowth curve as the only deviation from the idealized case. However, combinations of these processes taken together as illustrated by the black-dashed and green curves only indicate a possible ingrowth curve placement on the MIRC given that a different selection of input parameters can alter the relative magnitudes of non-ideal effects.

While the 4-isotope MIRC of Figs. 1 and 4 provides insight into how various processes can influence the isotopic signature in the cavity

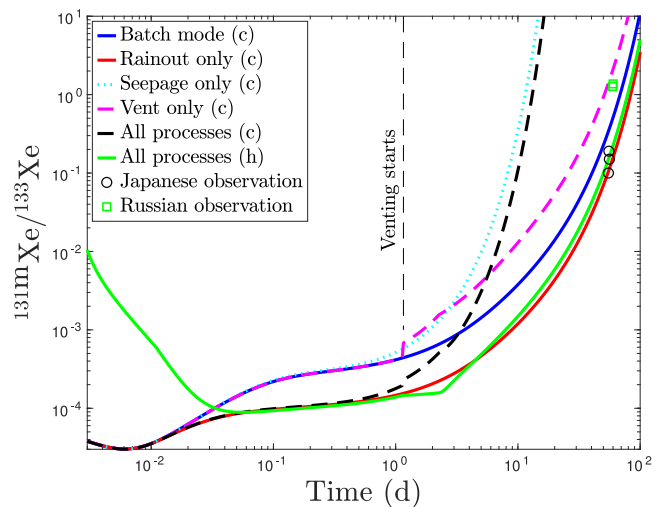


**Fig. 5.** Isotopic ratio of  $^{131\text{m}}\text{Xe}/^{133}\text{Xe}$  versus time since detonation. The same cases as plotted in Fig. 4 for xenon isotopic ratio correlation. Identification of the lines is the same as described in Fig. 4. (For interpretation of the references to color in this figure legend, the reader is referred to the web version of this article.)

Source: Replotted from Sun et al. (2023).

or subsurface containment zone, it is rarely useful owing to the very short half-life (9.1 h) of  $^{135}\text{Xe}$  resulting in loss of detectability in hours to several days depending on the level of subsurface and atmospheric dilution of the radioxenon signature. The ratio  $^{131\text{m}}\text{Xe}/^{133}\text{Xe}$  is far more persistent for measurement purposes and has been used to evaluate the 2013 DPRK UNE release up to 60 days after the detonation (Ringbom et al., 2014; Carrigan et al., 2016, 2020). Fig. 5 illustrates the evolution of this ratio for the same conditions considered in plotting Fig. 4. For comparison, the Japanese and Russian observations of the 2013 DPRK radioxenon signature are provided although no attempt has been made to match the conditions in the simulations with these observations. For additional details of both the Russian and Japanese atmospheric signature measurements and their interpretation please refer to Ringbom et al. (2014) and Carrigan et al. (2016). Although Figs. 4 and 5 provide insights into the deviation of isotopic ratios and ratio correlation from the reference case (well-mixed and closed cavity), deterministic models do not address the uncertainties of those parameters. For this reason, probabilistic models are needed.

### 3.2. Uncertainty of multi-parametric models

We consider the effects of uncertainty of the 4- and 2-isotope-ratio signatures based upon the 7,200 simulations having parameters covering the ranges shown in Table 1. Fig. 6 illustrates the zones of uncertainty created by plotting the isotopic ratios obtained from the simulations. At very early times, corresponding to the top region of the plot, the cavity-gas composition represented by the green zone spreads well beyond the England & Rider ingrowth curve due to uncertainty of independent yields responsible for radioxenon isotopes (Sloan et al., 2016). However, as time progresses, the region of uncertainty in the cavity-gas composition becomes wider crossing the England & Rider curve due to the rainout from the cavity to melt puddle and the seepage from the cavity to host rock. Gas seeping to the surface from the cavity produces the red zone which is shifted further away from the England & Rider result as well as from the discrimination line.

Fig. 7 shows the probability density functions representing the probability of obtaining isotopic gas concentration measurements at the surface as a function of time following an underground nuclear explosion. The bright color indicates regions of high probability where a particular isotopic ratio may exist at a given time while the dark

**Table 2**  
Sobol' total sensitivities.

Parameter	Cavity				Surface			
	$^{131m}\text{Xe}$	$^{133m}\text{Xe}$	$^{133}\text{Xe}$	$^{135}\text{Xe}$	$^{131m}\text{Xe}$	$^{133m}\text{Xe}$	$^{133}\text{Xe}$	$^{135}\text{Xe}$
Yield	8.28E-6	9.23E-5	1.99E-5	0.00	4.51E-2	7.39E-2	8.31E-2	1.00E-1
Rock type	2.12E-1	4.29E-1	2.62E-1	6.58E-1	1.64E-2	3.09E-2	2.44E-2	2.95E-2
Depth (burial)	9.11E-2	2.23E-1	1.66E-1	3.14E-1	6.02E-1	6.46E-1	7.75E-1	5.85E-1
Chimney ratio	0.00	0.00	0.00	0.00	9.62E-2	1.53E-1	1.74E-1	1.87E-1
Permeability	0.00	0.00	0.00	0.00	1.69E-1	2.08E-2	9.07E-2	2.56E-2
Saturation	4.70E-5	8.06E-4	1.84E-4	1.46E-7	8.18E-4	0.00	2.89E-4	0.00
Source temp	0.00	6.70E-6	0.00	0.00	0.00	0.00	0.00	0.00
Rainout rate	1.72E-3	1.10E-2	3.66E-3	5.94E-6	3.93E-3	1.85E-3	6.77E-3	5.10E-3
Diffusion rate	2.51E-3	1.37E-2	3.92E-3	4.87E-4	1.08E-3	2.26E-3	1.12E-3	2.07E-3
Seepage rate	6.12E-1	3.24E-1	5.64E-1	6.42E-2	5.65E-2	2.50E-1	1.58E-1	4.03E-1
IY uncertainty	5.54E-7	0.00	0.00	0.00	1.87E-3	0.00	2.33E-4	0.00

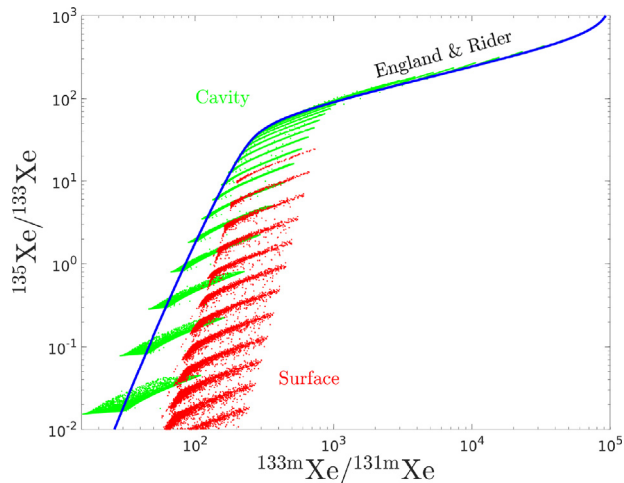


**Fig. 6.** Four-isotope plot illustrating effect of uncertainty resulting from the ranges of the eleven different parameters shown in Table 1. The blue curve corresponds to the England and Rider based model discussed previously. The solid/banded green zone corresponds to the ranges of uncertainty for gas compositions in the post-detonation cavity. The red-banded zone represents the range in isotopic ratios for gases that reach the surface. Note that the appearance of banding is a result of the parameter selection methodology. Banded zones should be interpreted as being contiguous. (For interpretation of the references to color in this figure legend, the reader is referred to the web version of this article.)

blue shows zones of essentially zero probability.  $^{131m}\text{Xe}$  remains a high signature strength after 50 days with high probability while  $^{133m}\text{Xe}$  and  $^{133}\text{Xe}$  signatures decay according to their half-lives. Due to the short half-life of  $^{135}\text{Xe}$ , its signature disappears rapidly during this timeframe.

It is not surprising that plots of the total xenon isotopic flux ( $\text{Bq s}^{-1}$ ) at the surface, shown in Fig. 8, have a similar appearance to Fig. 7 regarding the isotopic activity concentration. The values of the isotopic flux at the surface are necessary for predicting the probability of obtaining a particular composition of gases at the surface as represented in the four-isotope MIRC. The probabilistic output of xenon fluxes is a potential input into models of atmospheric transport.

When signal strength (for detectability) is defined as

$$f_i(\mathbf{x}) = \frac{1}{t} \int_0^t \log(c_i) dt, \quad i = 1, 2, 3, 4, \quad (1)$$

we conducted Sobol' sensitivity analyses for all four xenon isotopes both in the cavity and at the ground surface. In Eq. (1),  $x$  represents the 11-dimensional parameter space,  $t$  denotes the simulation time, and the index  $i = 1, 2, 3, 4$  represents  $^{131m}\text{Xe}$ ,  $^{133m}\text{Xe}$ ,  $^{133}\text{Xe}$ , and  $^{135}\text{Xe}$ , respectively. Table 2 of Sobol' total sensitivity indices (TSIs) indicates that the signal strength in the cavity is mainly determined by rock type and seepage rate while the strength at ground surface is influenced by the seepage rate and depth of burial. Initial rock saturation and the uncertainties of independent yields play only minor roles in xenon

signal strength.

The xenon signal strength  $f$  in the cavity and at ground surface is plotted against the dimension of rock type  $x_2$  and the depth of burial  $x_3$ , respectively, in Fig. 9 and Fig. 10. The  $f$  value in the cavity mainly depends on the rock type and the seepage rate as illustrated in Table 2 while the values at ground surface are determined by the depth of burial and seepage rate. In spite of other uncertain inputs, Fig. 9 intuitively shows the dependence of the  $f$  value on the rock type constant. Fig. 10 indicates that the  $f$  value at ground surface is inversely proportional to the depth of burial.

### 3.3. Application to UNE screening

The announced 2013 DPRK UNE, detected atmospherically more than 50 days after detonation, is probably the most studied event using IMS atmospheric sampling stations with detections in both Japan and Russia (Ringbom et al., 2014; Carrigan et al., 2016, 2020). While the amplitude of observed signatures is the primary indicator of this event for screening purposes, signature composition can provide secondary support for its origin. Before source-term processes and subsurface transport are considered, it is instructive to compare data of xenon isotopic ratios and their ratio correlation against the idealized reference case (well-mixed and closed system). As already mentioned, the long period between detonation and detection eliminates the possibility of using the four-isotope ratio plot. The two-isotope plot including atmospheric background observations prior to the detonation time (here 0) is shown in Fig. 11. Without considering uncertainties, the blue solid curve in Fig. 11 represents the reference case (*i.e.*, England and Rider curve). When uncertainties of independent yields are considered, the ratio of  $^{131m}\text{Xe}/^{133}\text{Xe}$  becomes uncertain as shown by the green area. As indicated by England and Rider (1994), the value of independent yields has an uncertainty exceeding 64%. If we double the IY uncertainties, which is a possibility indicated by England and Rider, the blue envelope displays the corresponding ratio uncertainty. For the purpose of screening, data points located in the green and/or blue envelopes may be considered as potential signatures produced by a UNE.

In addition to the reference ratio considering IY uncertainty  $x_{11}$ , we further consider the effect on UNE screening by utilizing our models of source-term processes and subsurface transport. Fig. 12a shows the uncertain ratio of  $^{131m}\text{Xe}/^{133}\text{Xe}$  considering 11-dimensional uncertain inputs ( $x_i$ ,  $i = 1, 2, \dots, 11$ ) in the cavity and at ground surface. Fig. 12b presents the uncertain ratio in host rock and at ground surface. Data points with specified sample locations that are located in corresponding envelopes may be from a UNE. For the sake of comparison, we include the ratio predictions from deterministic simulations of the detonation depth and rock type of the Barnwell and Disco Elm UNEs.

## 4. Conclusions and discussion

Xenon isotopic ratios and their correlations are derived using the closed-form solution of decay and ingrowth networks based on the

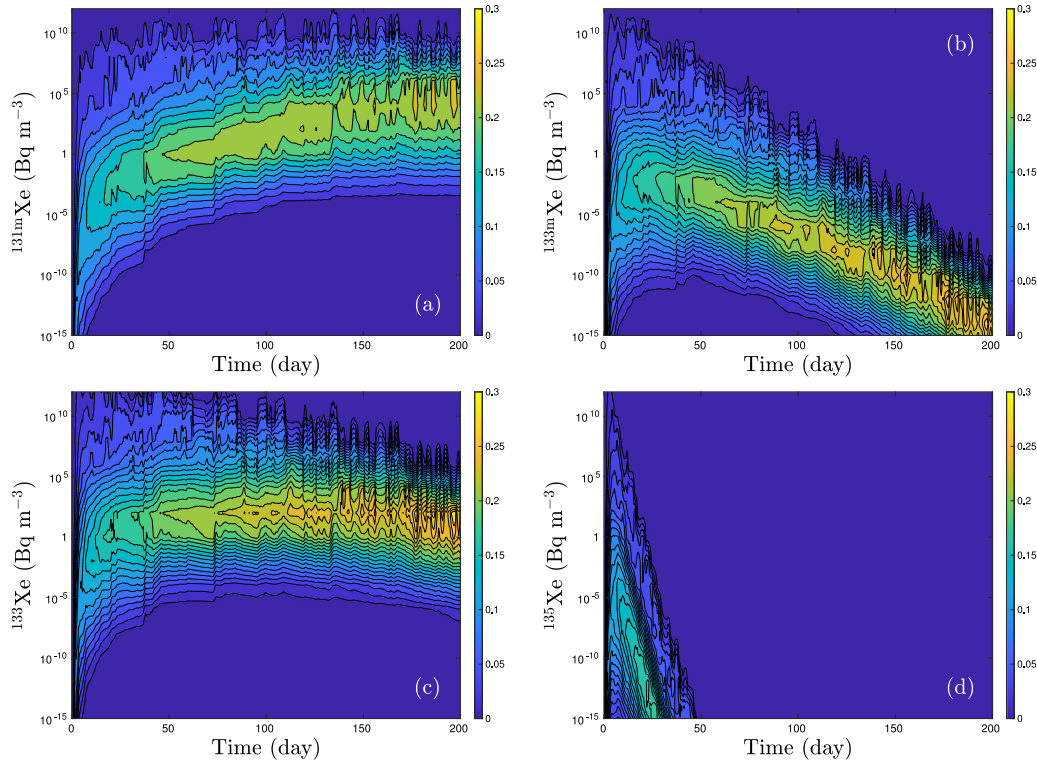


**Fig. 7.** Individual plots of the four radioxenon isotopes show the probability of measuring a given activity concentration of the gas at the surface of a containment zone as a function of time following detonation. Color scales to the right of the plots indicate the probability of each gas having a given concentration at a particular time. The rapid fall off with time of  $^{135}\text{Xe}$  illustrates the limited value of the four-isotope plot for screening signatures from UNEs over periods of more than a few days. (a)  $^{131\text{m}}\text{Xe}$ , (b)  $^{133\text{m}}\text{Xe}$ , (c)  $^{133}\text{Xe}$ , and (d)  $^{135}\text{Xe}$ . (For interpretation of the references to color in this figure legend, the reader is referred to the web version of this article.)

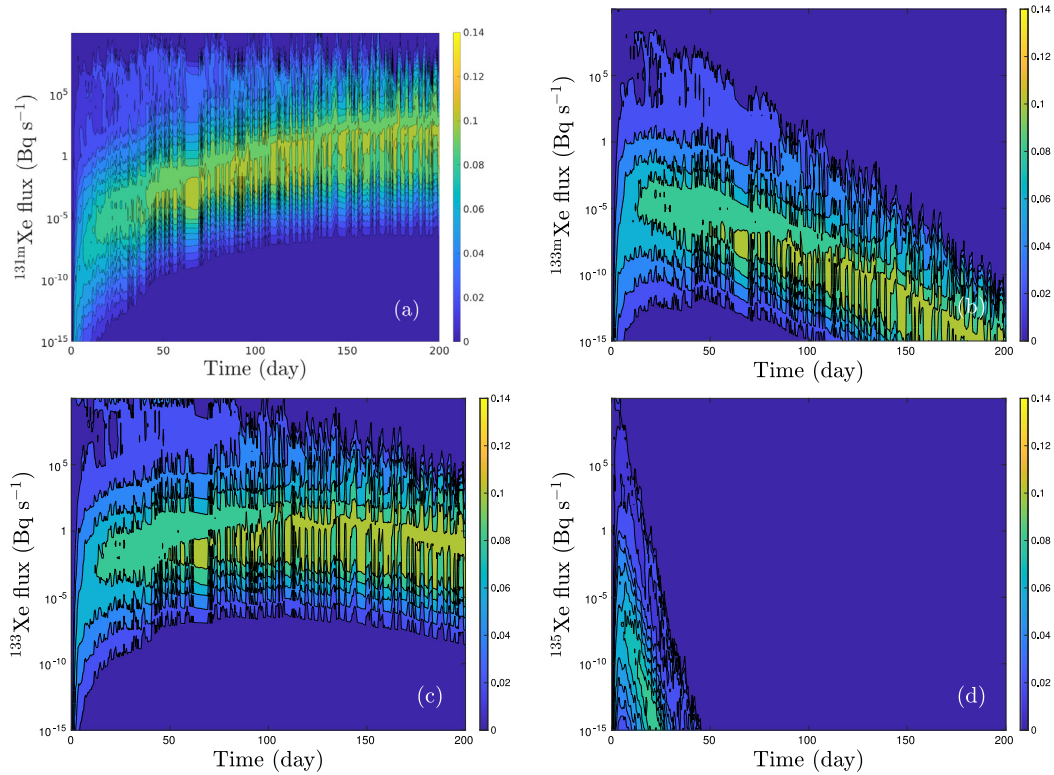


**Fig. 8.** Individual plots of the four radioxenon isotopes show the probability of measuring a given activity flux of the gas at the surface of a containment zone as a function of time following detonation. Color scales to the right of the plots indicate the probability of each gas having a given concentration at a particular time. (a)  $^{131\text{m}}\text{Xe}$ , (b)  $^{133\text{m}}\text{Xe}$ , (c)  $^{133}\text{Xe}$ , and (d)  $^{135}\text{Xe}$ . (For interpretation of the references to color in this figure legend, the reader is referred to the web version of this article.)

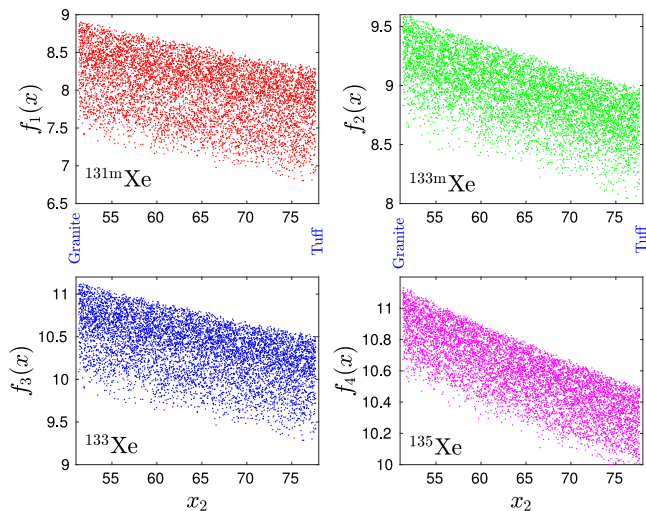


Fig. 9. Scatter plot of xenon signal strength in the cavity projected on rock type.

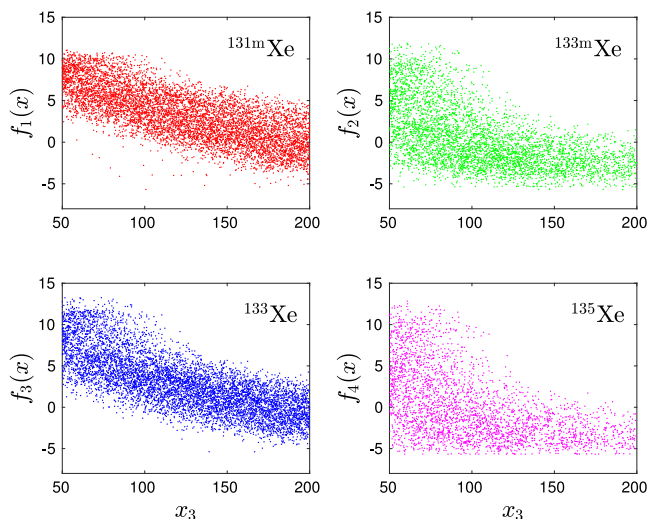


Fig. 10. Scatter plot of xenon signal strength at ground surface projected on the depth of burial.

assumption of a well-mixed and closed cavity. This scenario serves as the reference case for evaluating source-term processes and subsurface transport. Data points that closely align with the reference curve (Fig. 11) have been typically assumed to originate from a UNE. To account for uncertainties in independent yields, the reference curve is replaced by an area of uncertainty. Data points within this area can be quantitatively identified as potential signatures from a UNE.

When source-term processes (e.g., rainout, back diffusion, seepage, and venting) are taken into account, the locality-specific ratio envelope should be employed to more accurately screen for UNE signatures (Fig. 12). By coupling more realistic source-term activity models with subsurface transport models, we can derive probabilistic xenon concentrations at the ground surface and fluxes to the atmosphere. These insights will potentially help to guide onsite inspection and sampling efforts. The uncertain ratios and their correlations, derived from the probabilistic concentrations, represent more realistic screening tools to distinguish atmospheric UNE signatures from signatures associated with other nuclear sources (e.g., reactors and isotope production facilities).

UNE-related processes are complex, interdependent, and specific to both time and space (Sun and Carrigan, 2016; Carrigan et al., 2020; Bourret et al., 2021). The intricate physics of UNEs necessitates

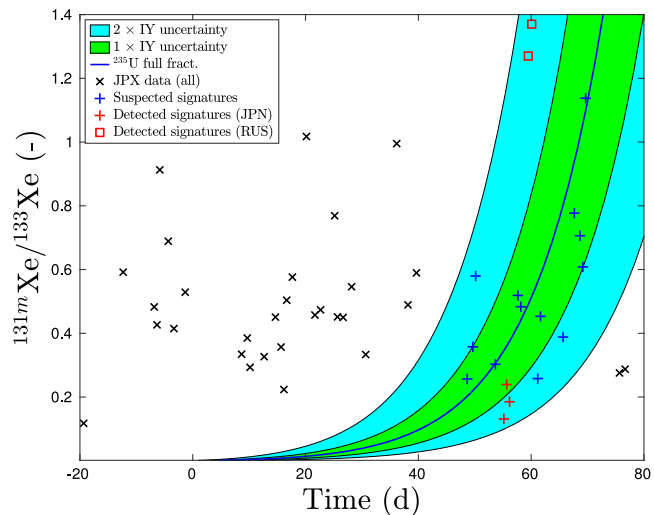


Fig. 11. Measurements of  $^{131\text{m}}\text{Xe}/^{133}\text{Xe}$  versus time obtained from a Japanese IMS atmospheric gas monitoring site (RN38) during the periods prior to and after the announced DPRK2013 UNE. The blue line corresponds to the ideal case of a closed, well-mixed cavity (also known as batch mode or England and Rider case) assuming decay products from U235 fission. The green zone is the result of uncertain independent yields from England and Rider (1994). The blue area bounds ratios that represent the doubled uncertainties in independent yields indicated by England and Rider. Both green and blue zones represent the uncertainty of the ratio in the cavity. (For interpretation of the references to color in this figure legend, the reader is referred to the web version of this article.)

high-fidelity models, which can be computationally expensive and impractical for timely decision-making in UNE inspection and monitoring. The post-detonation reactions that produce xenon isotopes in the cavity and melt puddle involve multiple precursors with complex branching (bifurcation) and converging (confluent) pathways. When source-term processes and multiphase transport are coupled with chain reactions, carrying out physics-based simulations becomes less feasible for timely evaluations of UNE events. To address this challenge, the physics-based models developed in this study are stored in model repositories. These repositories can be utilized to develop machine-learning models that screen UNE signatures more accurately and rapidly.

Finally, the UNE monitoring community should consider the potential use of non-traditional natural tracers to enhance the detection of radioxenon signatures during both atmospheric monitoring and on-site inspections. For instance, models developed by Pazdaniakou et al. (2024) suggest that water vapor may be emitted in sufficient quantities from the subsurface to be detectable by overhead satellites monitoring the infrared spectrum. However, further experiments are necessary to validate this concept. In the context of onsite inspections, natural and UNE-produced radon presents an alternative radionuclide that may be valuable for identifying a test site. Radon can indicate subsurface pressure anomalies associated with a UNE and allows for real-time monitoring, unlike xenon isotope measurements (Carrigan, 2013; Carrigan et al., 2022; Pazdaniakou et al., 2024).

#### CRedit authorship contribution statement

**Charles R. Carrigan:** Writing – original draft, Investigation, Conceptualization. **Yunwei Sun:** Writing – original draft, Investigation, Formal analysis, Conceptualization. **Eric B. Herbold:** Project administration, Funding acquisition. **Tarabay Antoun:** Project administration, Funding acquisition.

#### Declaration of competing interest

The authors declare that they have no known competing financial interests or personal relationships that could have appeared to influence the work reported in this paper.

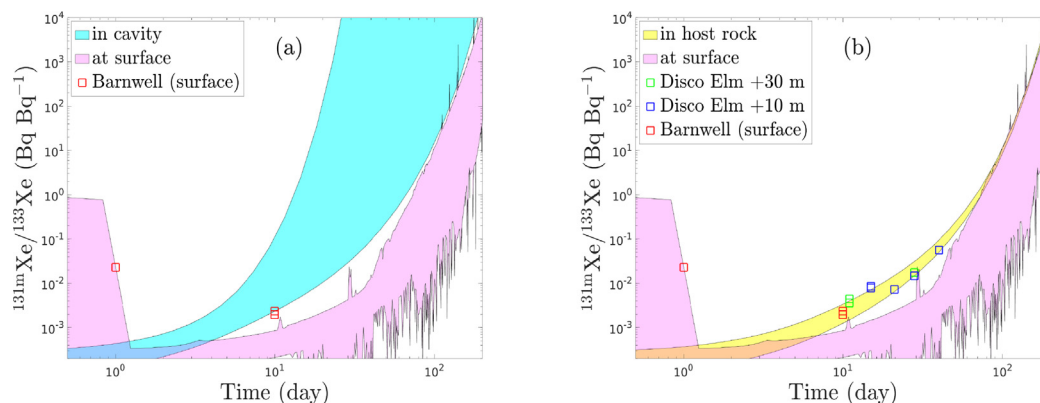


Fig. 12. Xenon isotopic ratio versus time with Disco Elm and Barnwell data. Uncertain isotopic ratio of  $^{131m}\text{Xe}/^{133}\text{Xe}$  (a) in the cavity and at ground surface (b) in host rock and at ground surface. (For interpretation of the references to color in this figure legend, the reader is referred to the web version of this article.)

## Acknowledgments

We thank anonymous reviewers for their constructive reviews and helpful comments leading to an improved manuscript. This research was funded by the National Nuclear Security Administration, United States, Defense Nuclear Nonproliferation Research and Development (NNSA DNN R&D), United States, U.S. Department of Energy, United States and performed under the auspices of the U.S. Department of Energy by Lawrence Livermore National Laboratory, United States under Contract number DE-AC52-07NA27344. The authors acknowledge important interdisciplinary collaboration with scientists and engineers from Los Alamos National Laboratory, Lawrence Livermore National Laboratory, Mission Support and Test Services, Pacific Northwest National Laboratory, and Sandia National Laboratories.

## Data availability

No data was used for the research described in the article.

## References

- Bourdon, B., Pili, E., 2023. Thermodynamic determination of condensation behavior for the precursory elements of radioxenon following an underground nuclear explosion. *J. Environ. Radioact.* 261, 107125.
- Bourret, S.M., Kwicklis, E.M., Miller, T.A., Stauffer, P.H., 2019. Evaluating the importance of barometric pumping for subsurface gas transport near an underground nuclear test site. *Vadose Zone J.* 18 (1), 180134.
- Bourret, S.M., Kwicklis, T.A., Stauffer, P.H., 2021. Evaluation of several relevant fractionation processes as possible explanation for radioxenon isotopic activity ratios in samples taken near underground nuclear explosions in shafts and tunnels. *J. Environ. Radioact.* 237, 106698.
- Butkovich, T.R., 1974. Rock Melt from an Underground Nuclear Explosion. University of California, Lawrence Livermore Laboratory Report UCRL-51554.
- Carrigan, C.R., 2013. Using background radon to optimize the ability to detect an underground nuclear explosion during an on site inspection. In: *Invited Presentation, Radon 2013 Conference*. Prague, Czechia, 2013, Lawrence Livermore National Laboratory, LLNL-ABS-641891.
- Carrigan, C.R., Sun, Y., Antoun, T., 2022. Evaluation of subsurface transport processes of delayed gas signatures applicable to underground nuclear explosions. *Sci. Rep.* 12 (13169), <http://dx.doi.org/10.1038/s41598-022-16918-5>.
- Carrigan, C., Sun, Y., Hunter, S., Ruddie, D., Wagoner, J., Myers, K., Emer, D., Drellack, S., Chipman, V., 2016. Delayed signatures of underground nuclear explosions. *Sci. Rep.* 6, 1–9. <http://dx.doi.org/10.1038/srep23032>.
- Carrigan, C.R., Sun, Y., Pili, E., Neuville, D., Antoun, T., 2020. Cavity-melt partitioning of refractory radionuclides and implications for detecting underground nuclear explosions. *J. Env. Radio* 219, 106269. <http://dx.doi.org/10.1016/j.jenvrad.2020.106269>.
- Cassata, W.S., Prussin, S.G., Knight, K.B., Hutcheon, I.D., Isselhardt, B.H., Renne, P.R., 2014. When the dust settles: stable xenon isotope constraints on the formation of nuclear fallout. *J. Environ. Radioact.* 137, 88–95.
- England, T.R., Rider, B.F., 1994. ENDF-349 Evaluation and Compilation of Fission Product Yields 1993. Los Alamos National Laboratory, LA-UR-94-3106.
- Hao, Y., Sun, Y., Nitao, J.J., 2012. Overview of NUFT – a versatile numerical model for simulating flow and reactive transport in porous media. In: Zhang, et al. (Eds.), *Ground water reactive transport model*. Bentham Science Publishers.
- Harp, D.R., Bourret, S.M., Stauffer, P.H., Kwicklis, E.M., 2020. Discriminating underground nuclear explosions leading to late-time radionuclide gas seeps. *Geophys. Res. Lett.* 47, e2019GL086654.
- Jordan, A.B., Stauffer, P.H., Knight, E.E., Rougier, E., Anderson, D.N., 2015. Radionuclide gas transport through nuclear explosion-generated fracture networks. *Sci. Rep.* 5 (18383).
- Kalinowski, M.B., Axelsson, A., Bean, M., Blanchard, X., Bowyer, T.W., Brachet, G., Hebel, S., McIntyre, J.I., Peters, J., Pistner, C., Raith, M., Ringbom, A., Saey, P.R.J., Schlosser, C., Stocki, T.J., Taffary, T., Ungar, R.K., 2010. Discrimination of nuclear explosions against civilian sources based on atmospheric xenon isotopic activity ratios. *Pure Appl. Geophys.* 167 (4–5), 517–539.
- Lowrey, J.D., Biegalski, S.R., Deinert, M.R., 2013. UTEX modeling of radioxenon isotopic fractionation resulting from subsurface transport. *J. Radioanal. Nucl. Chem.* 296 (1), 129–134.
- McKay, M.D., Beckman, R.J., Conover, W.J., 1979. A comparison of three methods for selecting values of input variables in the analysis of output from a computer code. *Technometrics* 21 (2).
- Medici, F., 2001. The IMS radionuclide network of the CTBT. *Radiat. Phys. Chem.* 61 (3–6), 689–690. [http://dx.doi.org/10.1016/S0969-806X\(01\)00375-9](http://dx.doi.org/10.1016/S0969-806X(01)00375-9).
- Nitao, J.J., 1998. User's Manual for the USNT Module of the NUFT Code, Version 3.0 (NP-Phase, NC-Component, Thermal). Lawrence Livermore Technical Report, UCRL-MA-130653-REV-2.
- Olsen, C.W., 1967. Time history of the cavity pressure and temperature following a nuclear detonation in alluvium. *J. Geophys. Res.* 72 (20), 5037–5041. <http://dx.doi.org/10.1029/JZ072i020p05037>.
- Pazdriakou, A., Mourzenko, V., Thovert, J.-F., Adler, P.M., Pili, E., 2024. Enhancing detection of underground nuclear tests with unconventional tracers. *Pure Appl. Geophys.* <http://dx.doi.org/10.1007/s00024-024-03595-w>.
- Plompen, A.J.M., Cabellos, O., De Saint Jean, C., et al., 2020. The joint evaluated fission and fusion nuclear data library, JEFF-3.3. *Eur. Phys. J. A* 56 (7), 181.
- Ringbom, A., Axelsson, A., Aldener, M., Bowyer, T.W., Fritioff, T., Hoffman, I., Khrustalev, K., Nikkinen, M., Popov, V., Popov, Y., Ungar, K., Wotawa, G., 2014. Radioxenon detections in the CTBT international monitoring system likely related to the announced nuclear test in North Korea on February 12 2013. *J. Environ. Radioact.* 128, 47–63.
- Saltelli, A., Ratto, M., Andres, T., Campolongo, F., Cariboni, J., Gatelli, D., Saisana, M., Tarantola, S., 2008. *Global Sensitivity Analysis*. John Wiley, The Primer. 663.
- Schulze, J., Auer, M., Werzi, R., 2000. Low level radioactivity measurement in support of the CTBTO. *Appl. Radiat. Isot.* 53 (1–2), 23–30. [http://dx.doi.org/10.1016/S0969-8043\(00\)00182-2](http://dx.doi.org/10.1016/S0969-8043(00)00182-2).
- Sloan, J., Sun, Y., Carrigan, C., 2016. Uncertainty quantification for discrimination of nuclear events as violations of the comprehensive nuclear-test-ban treaty. *J. Environ. Radioact.* 155, 130–139.
- Sobol', I., 1990. Sensitivity estimates for nonlinear mathematical models (in Russian). *Matematicheskoe Modelirovanie* 2, 112–118.
- Sun, Y., Buscheck, T.A., Hao, Y., 2012. An analytical method for modeling first-order decay networks. *Comput. Geosci.* 39, 86–97.
- Sun, Y., Carrigan, C.R., 2014. Modeling noble gas transport and detection for the comprehensive nuclear-test-ban treaty. *Pure Appl. Geophys.* 171 (3–5), 735–750.
- Sun, Y., Carrigan, C.R., 2016. Thermally driven advection for radioxenon transport from an underground nuclear explosion. *Geophys. Res. Lett.* 43, 4418–4425. <http://dx.doi.org/10.1002/2016GL068290>.
- Sun, Y., Carrigan, C., Cassata, W., Hao, Y., Ezzedine, S., Antoun, T., 2021. A closed-form solution for source-term emission of xenon isotopes from underground nuclear explosions. *Transp. Porous Med.* 139, 131–153. <http://dx.doi.org/10.1007/s11242-021-01650-x>.

Sun, Y., Carrigan, C.R., Hao, Y., 2015. Radioxenon production and transport from an underground nuclear detonation to ground surface. *Pure Appl. Geophys.* 172, 243–265.

Sun, Y., Carrigan, C.R., Pili, E., Antoun, T., 2023. Implications of underground nuclear explosion cavity evolution for radioxenon isotopic composition. *Pure Appl. Geophys.* 180, 1395–1406.

Tong, C., 2005. *PSUADE User's Manual*. Lawrence Livermore National Laboratory, LLNL-SM-407882.